PCCP

Accepted Manuscript

ROYAL SOCIETY OF CHEMISTRY

www.rsc.org/pccp

Cite this: DOI: 10.1039/c0xx00000x

www.rsc.org/xxxxxx

ARTICLE TYPE

Construction of High Efficiency Non-doped Deep Blue Emitter Based on Phenanthroimidazole: Remarkable Substitution Effects on the Excited State Properties and Device Performance

Zhiming Wang*[a], Ying Feng[a], Shitong Zhang[b], Yu Gao[b], Zhao Gao[b], Yanming Chen[a], Xiaojuan Zhang[a], Ping Lu[b], Bing Yang[b], Ping Chen*[c], Yuguang Ma[b], Shiyong Liu[c]

Received (in XXX, XXX) Xth XXXXXXXXX 20XX, Accepted Xth XXXXXXXXX 20XX
DOI: 10.1039/b000000x

Aryl-substituted phenanthroimidazoles (APIs) are beneficial due to their facile synthesis, thermal properties, high quantum yields, exciton efficiencies by reverse intersystem crossing (RISC) process. However, it is puzzled that how to combine high quantum yields, exciton utilizing ratios and color purity with stable blue-emitting compounds via coupling. Here, **BPPI** and **N-BPPI** are utilized as model compounds for understanding *C2*- and *N1*-substitution effects via constructing dimers in each coupling position. By integrating the information obtained from DFT calculations, photophysical analysis, and OLED performance, valuable guidance was obtained. *C2*-substituted groups typically offer a large orbital overlap between the LE states with large oscillator strengths, and play an important role in the maximum peak area and quantum yields. *N1*-substituted groups contribute to enhanced orbital coupling and cause excitons to transform freely between different excited states. Unexpected results from the decreased barriers of the *N1*-coupled system included the loss of PL efficiency and increased emission spectra width, which are important for efficiency and color purity of deep blue emitters. The substitution effects are consistent with most reported results. Therefore, this work may be useful for the generation of non-doped deep blue electroluminescent API-based materials.

1. Introduction

Organic light-emitting devices (OLEDs) have attracted considerable attention due to their potential applications in full-color flat panel displays. [1,2] Till date, owing to the rapid improvement in OLED performance, many efficient fluorescent and phosphorescent emitters have emerged. However, some issues remain to be addressed, including the lack of stable deep-blue-emitting materials with high quantum yields, high exciton utilizing ratios, and high color purity (3H-type) for practical industrial applications. [3]

Recently, aryl-substituted phenanthroimidazoles (APIs) have attracted tremendous attention as efficient blue-emitting building blocks due to their simple synthesis, excellent thermal properties, high fluorescence quantum yields, and "bipolar" properties. [4-9] More importantly, a unique emission process is found in some APIs derivatives, such as thermally-activated delayed fluorescence (TDAF) or hybridized local and charge-transfer (HLCT) excited state, which rapidly converts triplet excitons to singlet excitons through reverse intersystem crossing (RISC) before populating on the long lifetime and T state with higher energy. This excited state conversion could enhance the exciton utilizing efficiency (EUE) and avoid triplet exciton depopulation caused by concentrate quenching, breaking through the radiative exciton ratio of 25% of spin statistics. [10-12]

Viewing API-based materials in HLCT from our previous reports, their emissive states should be a combination of a large transition moment from the locally excited state (LE) and a small binding energy of the charge transfer (CT) states. [10,11] The former contributes to highly efficient fluorescence radiative decay arising from larger transition moments with large orbital overlaps, while the latter offers an efficient conversion channel and guarantees a high fraction of singlet exciton generation. Using this combined state as an emissive state, it is possible to obtain an ideal emitter with efficient performance and EUE through the use of singlet and triplet excitons in OLEDs. However, it is a challenge to construct the proper CT state in wide band-gap emitters with high color purity (CIE x+y<0.3). [11-13]

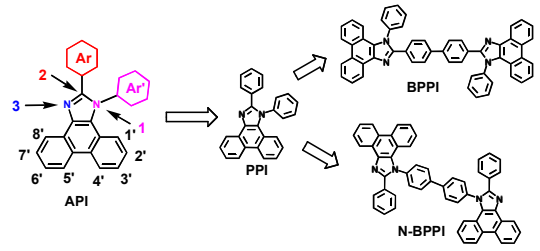

Scheme 1. The structures of API, PPI, **BPPI** and **N-BPPI.**

Operational guidance regarding structure-property relationships, such as substitution effects, is often desired. In APIs, there are two important substitution positions, namely the *N1* and *C2* in the imidazole ring, and some derivatives are reported to exhibit excellent performances as emitters or hosts. [4-9, 10]

In our previous report, 4,4'-bis(1-phenyl-phenanthro[9,10-d]imidazol-2-yl) biphenyl (**BPPI**) was coupled with a peripheral phenanthroimidazole (PI) group and a biphenyl center at the *C2*-position of API and was reported to be a blue-emitting material with superior performance in simple non-doped devices (as shown in **Scheme 1**), but the emission color was located at unexpected sky-blue area. [4] Here, we describe our attempts to move the biphenyl center to the *N1*-position and obtain a **BPPI** derivative known as **N-BPPI**. The two isomers were compared following this adjustment, and the effects of the coupling position on the excited-state properties and device performance were discussed in order to give operational guidance regarding the structure-function relationships of the compound.

The isomeric oligomers were synthesized via a one-pot reaction and Suzuki coupling reaction. Moreover, they exhibited ideal thermal stabilities, high fluorescent efficiencies, proper energy levels, and a HLCT state with intercrossed LE and CT characteristics. Furthermore, the non-doped OLEDs exhibited good performance and deep blue emission with CIEs of (0.15, 0.13) and (0.15, 0.08) for **BPPI** and **N-BPPI**, respectively. A detailed comparison of the DFT calculations, the photophysical and device analysis gave some information regarding the relationship between the coupling position and fluorescence quantum yields, exciton utilizing efficiency, and color purity. Herein, we present our detailed experimental evidence and theoretical analysis.

2. Experimental Section

All the reagents and solvents used were purchased from Aldrich or Acros and used as received. All reactions were performed under a dry nitrogen atmosphere. The NMR spectra were recorded on an AVANCZ 500 spectrometer at 298 K by utilizing deuterated chloroform (CDCl3) or dimethyl sulfoxide (DMSO) as solvents and tetramethylsilane (TMS) as an internal standard. Elemental analysis was performed on a Flash EA 1112 CHNS-O elemental analysis instrument. MALDI-TOF-MS mass spectra were recorded using an AXIMA-CFRTM plus instrument. UV-vis absorption spectra were recorded on a UV-3100 spectrophotometer. Fluorescence measurements were carried out with a RF-5301PC. Differential scanning calorimetry (DSC) analysis was carried out using a NETZSCH (DSC-204) instrument at 10 °C min^{-1} under nitrogen. Cyclic voltammetry (CV) was performed with a BAS 100W Bioanalytical System, using a glass carbon disk (F = 3mm) as the working electrode, a platinum wire as the auxiliary electrode with a porous ceramic wick, and a Ag/Ag+ as the reference electrode standardized by the redox couple ferricinium/ferrocene. All solutions were purged with a nitrogen stream for 10 min prior to the measurements. The procedure was performed at room temperature and a nitrogen atmosphere was maintained during the measurements.

3. Device fabrication

The EL devices were fabricated by vacuum deposition of the materials at 10^{-6} Torr onto ITO glass with a sheet resistance of 25 Ω square-1. All organic layers were deposited at a rate of 1.0 Å s^{-1}. The cathode was deposited with Mg and Ag at a deposition rate of 0.1 Å s^{-1}. The electroluminescence (EL) spectra and CIE coordination of these devices were measured using a PR650 spectra scan spectrometer. The luminance-current and density-voltage characteristics were recorded simultaneously with the measurement of the EL spectra by combining the spectrometer with a Keithley model 2400 programmable voltage-current source. All measurements were carried out at room temperature under ambient conditions.

4. Synthesis and characterization

4.1 Synthesis and Basic Properties

The key step in the synthesis of APIs derivatives is a one-pot reaction between phenanthrenequinone or its derivatives, and the corresponding aromatic aldehyde, aromatic amine, or ammonium acetate. [4, 14] Various structures can be conveniently built by simply tuning the reactants. The respective precursor of **BPPI** or **N-BPPI** was synthesized in this manner by commercially available products, and was coupled via Suzuki coupling to afford the terminal materials in good yields (over 80%) as depicted in **Scheme S1**. Spectroscopic characterizations were carried out for both compounds, and the data corresponded well with their respective structures (As shown in **Figure.1** and **Figure. S1**).

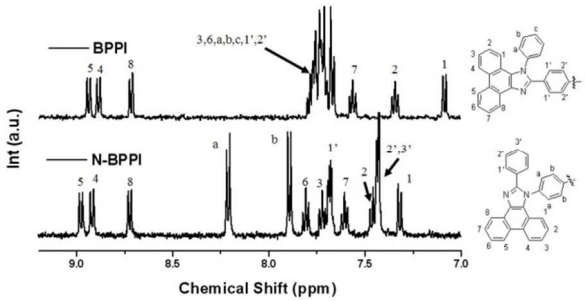

Figure 1. 1H NMR spectra of **BPPI** and **N-BPPI** in the aromatic range**.**

Similar thermal stabilities at the decomposition temperatures (5% weight loss, Td) for **BPPI** (552 °C) and **N-BPPI** (550 °C) indicated that the coupling position had little effect on the thermal stability of the compounds. Owing to their similar dimeric structures and symmetry, similar glass transition temperature (T_g, 195 °C) and crystallization behaviors were observed and were much higher than that of PPI (62 °C), indicating that dimeric PPI can effectively enhance the thermal stability of APIs derivatives, as shown in **Figure S3**. Such high T_gs are very rare in pure organic compounds, which implies that these compounds could forme morphologically stable films under Joule heating. [15] Atomic Force Microscope (AFM) measurements showed that the films exhibited fairly smooth surface morphologies with a roughness less than 0.5 nm, and were nearly unchanged after annealing at 120 °C for 2 h (shown in **Figure. 2**). These results indicated that the compounds could form very stable and smooth films to support EL device fabrication. [16]

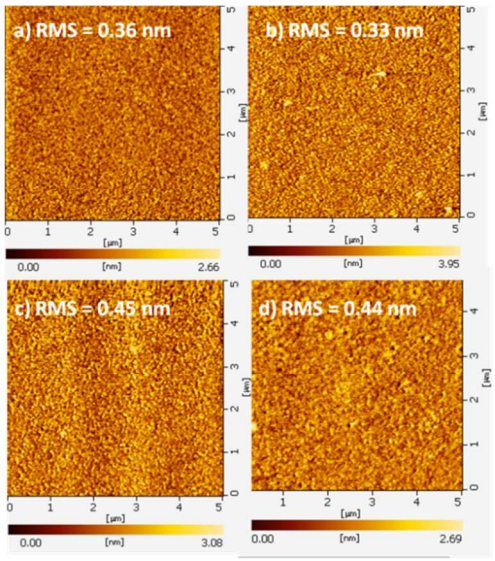

Figure 2 BPPI and **N-BPPI** film on a quartz plate at room temperature (a:**BPPI**, c: **N-BPPI**) and after annealing at 120oC for 2 h (b: **BPPI**, d: **N-BPPI**).

Table. 1 The basic properties of **PPI**, **BPPI** and **N-BPPI**.

	T_g (°C)	T_d [a] (°C)	PL λ_{max}/Φ_{fl} [b] (soln)	PL λ_{max}/Φ_{fl} [c] (film)	HOMO [d] (eV)	LUMO [d] (eV)
PPI	62	317	369/0.70	395/0.35	-5.53	-2.07
BPPI	195	552	418/0.92	448/0.85	-5.47	-2.29
N-BPPI	195	550	388/0.65	400/0.30	-5.59	-2.34

a. The temperature for 5% weight loss of the oligomers. b. The fluorescence quantum yield in solution using 0.5 M H2SO4 solution of quinine as reference (0.54). c. The solid state film was obtained by vacuum deposition on the quartz plate. d. Calculated by comparing with ferrocene (Fc) (4.8 eV) and calibrated using E1/2 (Fc/Fc+) measurement.

HOMO and LUMO levels were calculated from cyclic voltammetry. [17] As depicted in **Figure S4**, **N-BPPI** exhibited an onset potential of 0.98 V in the positive potential region, and its HOMO level was estimated to be -5.59 eV, a slight positive shift from that of **BPPI** (-5.47 eV). In the negative potential region, a quasi-reversible redox wave was observed, and potential bipolar applications for **N-BPPI** were estimated. The onset reduction potential was -2.34V vs Ag wire, and the LUMO level of **N-BPPI** was calculated to be -2.34 eV, revealing that the electron injection ability of **N-BPPI** was a little better than that of **BPPI** (-2.29 eV).

2.2 Theoretical Calculations

In **BPPI** and **N-BPPI**, there are three key twist angles (TA), which play important roles in the π-electron overlap of the frontier molecular orbitals and distributions in the excited state, namely the *N1*-TA (between the PI plane and the phenyl group attached to the *N1*-position), *C2*-TA (between the PI plane and the phenyl group attached to the *C2*-position), and B-TA (between two phenyl groups in the biphenyl center). As shown in **Figure 3a-b**, DFT calculations were carried out at the B3LYP/6-31G (d, p) level to determine the optimized structures. The TAs are listed in **Table S2**, and the differences in the TAs between **BPPI** and **N-BPPI** were quite small.

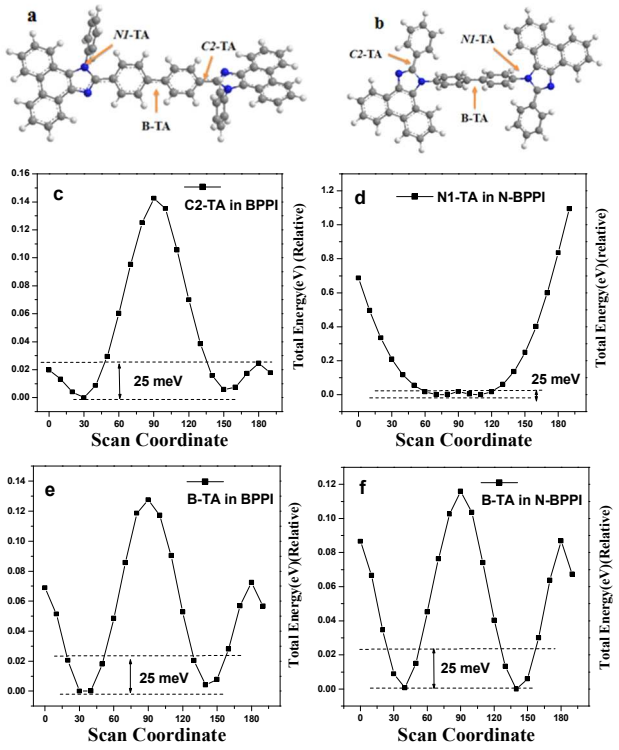

Figure 3. a-b) The optimized structures of **BPPI** and **N-BPPI** from DFT calculations; c-f) the ground state potential energy scan of both at different twist angles of biphenyl and the corresponding substituted position in the gas phase (using the CAM-B3LYP method and full geometrical optimization at each twist angle)

Due to the strong steric hindrance between neighboring hydrogen atoms, the *N1*-TA was nearly 80°, and the substituted group was nearly perpendicular to the PI plane. The ground state energy results by scanning different twist angles showed that the *N1*-TA was only limited at 60°-120° at room temperature (k_BT, 25 meV), or would rise steeply when the TA was out of this range (as shown in **Figure 3-d**). Therefore, the degree of conjugation at these angles was very limited, and the wave function of two PI moieties exhibited a relatively small overlap by the biphenyl bridge in the *N1*-position. The *C2*-TA and B-TA were located at about 30° (**Figure 3c** and **3e-f**), implying a large enough π-electron overlap between the *C2*-group and PI plane or two phenyl groups in the biphenyl center. [18]

In order to examine the excited-states of **BPPI** and **N-BPPI**, the natural transition orbitals (NTOs) for the $S_0 \rightarrow S_n$ (n=1-10) excitations were evaluated at the level of TD-ωB97X/6-31G (d, p) using the geometry of the S_0 state, as shown in **Figure 4** and **Figure S5-6**. [19] For the S0→S1 excitation in **BPPI**, the "hole" was primarily located on the entire molecule with the exception of the *N1*-phenyl moiety, while the "particle" was localized on the biphenyl moiety with a small fraction on the PI moiety. [10] This distribution implied the S_1 contained a major part of the LE transition of the biphenyl moiety and a minor part of the CT transition from the PI to the biphenyl unit, corresponding to the aforementioned HLCT. A homologous situation was observed in other excitations such as the $S_0 \rightarrow S_2$ transition. Its HLCT was composed primarily of the CT and the LE to some extent. Importantly, the $S_0 \rightarrow S_1$ transition exhibited a larger oscillator

strength ($f_{S0\rightarrow S1}$=2.3434) than $S_0\rightarrow S_2$ ($f_{S0\rightarrow S2}$=0.0021) or other $S_0\rightarrow S_n$ excitations, as a result of the major LE character in the HLCT state of **BPPI** (**Table 2**), which is necessary for high efficiency fluorescence. [10a]

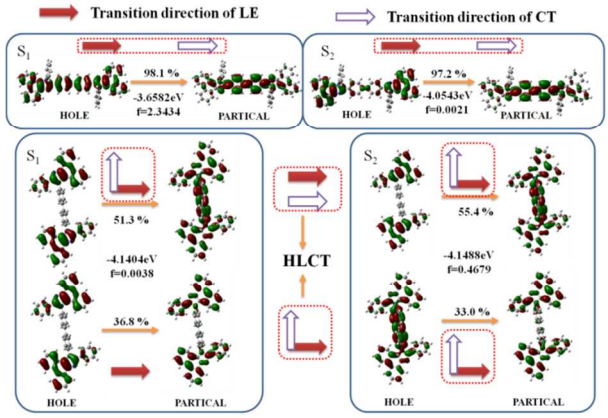

Figure 4. $S_0\rightarrow S_1$ and $S_0\rightarrow S_2$ NTO transition of **BPPI** and **N-BPPI** and the transition direction of LE or CT or mixed excited-state.

Table. 2. Calculated energy levels and oscillator strengths of **BPPI** and **N-BPPI** from NTO.

BPPI States	Energy(eV)	Oscilator Strength	**N-BPPI** States	Energy(eV)	Oscilator Strength
S1	-3.6582	2.3434	S1	-4.1404	0.0038
S2	-4.0543	0.0021	S2	-4.1488	0.4679
S3	-4.1855	0.0456	S3	-4.1765	0.0912
S4	-4.2657	0.0147	S4	-4.1860	0.0000
S5	-4.5284	0.0705	S5	-4.4296	0.0030
S6	-4.5772	0.0055	S6	-4.4401	0.4533
S7	-4.6819	0.0039	S7	-4.7532	0.0006
S8	-4.6872	0.0288	S8	-4.7581	0.2516
S9	-4.8052	0.0000	S9	-4.8783	1.4764
S10	-4.8460	0.0366	S10	-4.9391	0.0034

In **N-BPPI**, the "hole" and "particle" were more complicated than in **BPPI**. Every excitation in ten NTOs contained two transition configurations with close contributions; the one squint towards the LE state and the other was like the HLCT state described above (**Figure 4**). These results implied that **N-BPPI** exhibited a better mixed LE and CT state than **BPPI**, and the LE state dominated the fluorescence. In **BPPI**, the transition direction of the LE, CT, or mixed excited states were all of the same orientation along the *C2*-sbustitued direction, as the arrow shown in **Figure 4**. However, in **N-BPPI**, a given intersection angle appeared between two directions in the imidazole ring, namely one along the *C2*-substituted direction and another along the *N1*-substituted direction. Most of the CT component was nearly perpendicular to that of the LE in the same mixed transition configuration, which was a special excited state of D-A structure at the *N1*-position, perhaps. [10b, 14a]

This novel mixed state in **N-BPPI** led to low oscillator strengths, such as the $f_{S0\rightarrow S1}$ value of 0.0038, and the transition energy barrier was very little from S_1 to S_4 (0.04 eV). Such slight differences usually cause stronger orbit coupling leading to free exciton transformations between the four excited states at room temperature, and the emission species change or the number increases with changes in the external environment, such as thermal activation. This internal conversion (IC) between different excited states would cause the nonradiative decay ratio to increase in photoluminescence, and the efficiency would become lower than the absolute advantage transition of $S_1\rightarrow S_0$ with larger oscillator strength, which is confirmed by the optical measurements described below.

A similar phenomenon was observed previously in a comparison of TPM and TPMCN. [10b] TPMCN has a cyano group at the *N1*-phenyl of TPM, and was introduced as a class HLCT model compound with a higher EUE. In TPM, the $f_{S0\rightarrow S1}$ value was 1.168, which was significantly larger than the $f_{S0\rightarrow S2}$ (0.0297) and other $f_{S0\rightarrow Sn}$ (n=3-10) values, so the PL efficiencies were as high as ~90% in THF and ~35% in film. After inserting the cyano group, the oscillator strength of $S_0\rightarrow S_1$ was calculated to be 0.2327, which was even smaller than that of the $S_0\rightarrow S_2$ (0.8902). As such, the PL efficiency decreased to 10% in solution and 13% in film, respectively. However, the strong interstate transfer or perpendicular transition configuration of the CT component was not all bad; the closely distributed states led to easier exciton conversion, including the RISC process from triplet excitons to singlet excitons, so the EUE was improved to 85% in TPMCN from 16% in TPM.

2.3 Properties of Ground and Excited States

The UV and PL spectra were investigated to understand the ground and excited state properties (**Figure 5**). In the solution or state UV spectra, there was a strong, sharp absorption peak at 260 nm, the typical π-electron response of the phenanthrene derivative. [15a] Due to the extended π-electron delocalization by the biphenyl-bridge at the *C2* position, the π-π* electronic transition of **BPPI** exhibited a wide absorption peak around 365 nm in diluted THF. However, **N-BPPI** showed a strong absorption peak at about 280 nm with some small peaks until 370 nm. The 85 nm blue shift in **N-BPPI** absorption peak from **BPPI** is owing to the limited π-electron delocalization due to the larger *N1*-TA value. While the other small peaks were assigned to weak absorption vibrations, such as the *C2*-phenyl response at 360 nm like **PPI**. [4a] There was not an obvious wide CT band in the single molecule spectra, implying that the CT state radiative ratio was very low in the ground state. [11] In the film, **BPPI** exhibited a broad absorption band around 450 nm when the film thickness was 30 nm. This red-shift was due to enhanced inter or intra-molecule CT, such as *C2*-dihedral angle planarization effects or π-π aggregation. There was no change in the **N-BPPI** film with the same thickness, illustrating that the aggregation had little effect on its ground state.

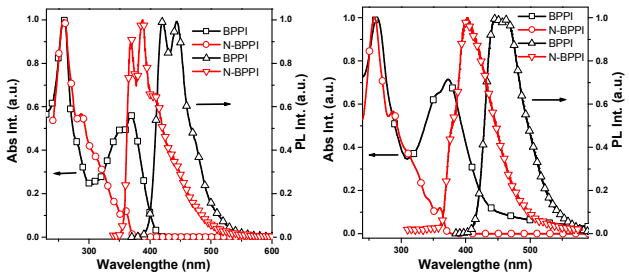

Figure 5. Abs. and PL spectra of **BPPI** and **N-BPPI** in solution (a) and film (b).

Vibronic fluorescence peaks (sharp bands) in both compounds were observed in solution, and suggested that strong CT processes were limited in transition. This low CT property is beneficial for high efficiency fluorescence emitters, so the fluorescence quantum yields were estimated to be ~92% for **BPPI** and 62% for **N-BPPI**. The value decreas from **BPPI** to **N-BPPI** may be due to the energy lost via nonradiative decay in the orbit coupling process as predicted via DFT. As compared to TPM (~90%) and TPMCN (~10%), the decrease is acceptable in quantum yields, which was might be related to the weak CT state between PI and the biphenyl center.

Meanwhile, the main peak of **N-BPPI** in THF at 388 nm was blue shifted as compared to that of **BPPI** at 418 nm, and was near that of **PPI** at 369 nm. This seemed very reasonable because **PPI** and **N-BPPI** have benzene at the *C2*-substituted position, which was the location of the LE state of **N-BPPI** in our simulation. In other words, the emission color of the API block may be more sensitive to the *C2*-substituted group than other positions. [4, 9] In the film spectra, **N-BPPI** showed a blue emission peak at 400 nm, whereas **BPPI** exhibited a peak at 448 nm and **PPI** exhibited a peak at 395 nm. Therefore, the fluorescence color can be controlled by simple chemical modification in *C2*-attached group of APIs, and most reported compounds have confirmed this conclusion as well. [4d, 13]

Unlike **BPPI**, which was red shifted by 30 nm in the film state, **N-BPPI** also exhibited fine vibronic fluorescence in film, which was red shifted by about 12 nm in solution. This difference can be attributed to two potential reasons: the increase of π-electron delocalization at the *C2*-position in the solid state, and the intersection angle difference of the transition direction of the LE and CT excited states. Additionally, the larger space volume of **N-BPPI** also played a role in inhibiting intermolecular interactions, thus not forming a more condensed molecular packing. In a word, it is a good choice to controlling a red shift in emission from the solution to solid state by extending the *N1* conjugated system, which may be useful for constructing deep blue emitters.

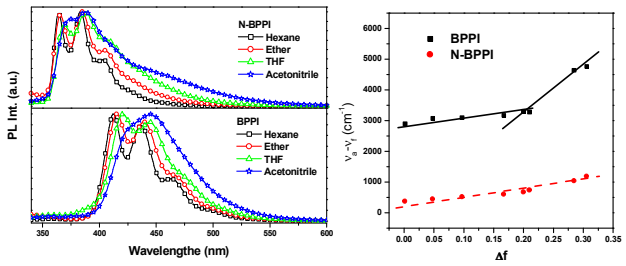

Figure 6. a) Solvatochromic fluorescence in solvents with increased solvent polarities. b) Linear correlation of orientation polarization (*f*) of solvent media with Stokes shift (ν_a-ν_f) for **BPPI** and **N-BPPI**.

To discuss the essential differences in the excited states of the compounds originating from the different coupling positions, solvatochromic effects were examined using eight solvents with increasing polarities, without hydrogen bond or π-π interactions between the solvent and single molecule (**Figure 6**). [19, 20] When the solvent polarity increased gradually from hexane to acetonitrile, **BPPI** exhibited an obvious red shift of 33 nm from 412 nm. This solvatochromic shift indicated that **BPPI** possessed a CT-emitting character in the fluorescent dipole moment of the CT state. However, in **N-BPPI**, the main fluorescent peaks, namely the peak at 363 nm in hexane and the peak at 374 nm in acetonitrile, were red shifted only 11 nm. While the intensity of the lower-energy emission band was strongly enhanced, and the full-width at half-maximum (FWHM) became more broad. The solvatochromic effect difference in **BPPI** and **N-BPPI** originated from the intersection angles of the transition directions in the LE and CT states as hypothesized by DFT, namely from the same orientation in **BPPI** to the perpendicular orientation in **N-BPPI**.

In addition, compared to the shift in **BPPI** from hexane to acetonitrile, the broaded spectra in **N-BPPI** had some relationship with the oscillator strength value of S1 state. In **N-BPPI**, the value was too low to dominate, and would be leading to the other excited states influenced with increasing solvent polarities, and then the spectra became broader as well. While, the increased FWHM influences the purity of the emission color, especially for deep blue emitters with the CIE valus at a rang of x+y<0.3. [4d, 13]

$$\mathrm{hc}(\nu_a - \nu_f) = \mathrm{hc}\left(\nu_a^0 - \nu_f^0\right) + \frac{2(\mu_e-\mu_g)2}{a_0^3} f(\varepsilon, n) \quad (1)$$

Equation. 1. Lippert-Mataga equation. h is the Plank constant, c is the speed of light in a vacuum, $f(\varepsilon, n)$ is the orientational polarizability of the solvents and $f(\varepsilon, n) = \left[\frac{\varepsilon-1}{2\varepsilon+1} - \frac{n^2-1}{2n^2-1}\right]$, $\nu_a^0 - \nu_f^0$ is the Stokes shifts when f is zero, a_0 is the solvent Onsager cavity radius, μ_e and μ_g are the dipole moments of excited-state and ground-state, respectively. ε is the solvent dielectric constant and n is the solvent refractive index. a_0 and μ_g are estimated at the level of b3lyp/6-31g(d,p) from the Gaussian09 package.

The dipole moment of the S1 state can be estimated from the slope of the plot of the Stokes shifts (ν_a-ν_f) against the solvent parameters $f(\varepsilon,n)$ (or the orientation polarizability) according to the Lippert-Mataga equation shown in **Equation 1** (for details see **Supporting Information**). [19]

The fitted results reflect a non-linear relationship between the Stokes shift and solvent polarity, as shown in **Figure 6b**. Two independent slopes of the fitted line suggested the existence of two different excited-states in **BPPI**, whose dipole moment (μ_e) was calculated to be 20.6 D in highly polar solvents (slope=14721, r=0.99) and 7.80 D in less polar solvents (slope=2093, r=0.90). The μ_e of 7.80 D could be attributed to the usual excited-state, which was a class LE-like state. The large μ_e of 20.6 D should be treated as a CT-like state, whose value was very close to the typical CT molecule DMABN with a μ_e of 23 D. [19b] The fluorescent solvatochromic experiments and nonlinear relationship between the Stokes shift and solvent polarity indicated that **BPPI** possessed an intercrossed LE and CT excited state with a HLCT state similar to TPA-NZB. [13a] On the other hand, **N-BPPI** exhibited simple linearity (slope=3177, r=0.94), which represented a single emitting species with a μ_e of 9.61 D. [19b, 20] This value was slightly larger than that of typical LE emitters, implying that a small part of the CT component was contained in the S1 emissive state of **N-BPPI**. The results illustrate that the CT effect on the S1 state from the same D-A structure, the substituted group at the *C2*-coupling position has a more obvious effect than the *N1*-coupling position.

2.4. Electroluminescence Properties

To investigate the EL properties, we constructed non-doped blue electroluminescent devices with respect to their appropriate energy levels. The multilayered structures were fabricated as ITO/MoO_x(2 nm)/NPB (40 nm)/**BPPI** or **N-BPPI** (50 nm)/Mg:Ag (10:1 by weight, 100 nm), in which MoOx and NPB were employed as the carrier-modified layers. [21] As shown in **Figure 4**, the EL spectra of both emitters showed saturated deep blue emission with CIE coordinates of (0.15, 0.13) for **BPPI** and (0.15, 0.08) for **N-BPPI**, which were stable in the drive voltage range from 5V to 12V.

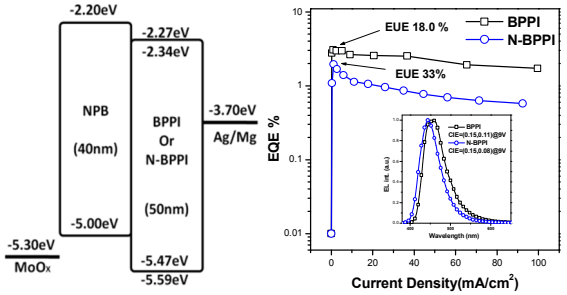

Figure 7. a) The EL structure of the device; b) the external efficiency versus current-density curve in device. Inset: EL spectra and their CIE @ 9V

$$\eta_{EL} = \eta_{rec} \times \eta_s \times \eta_{PL} \times \eta_{out} \qquad (2)$$

Equation 2. The relationship between EQE and EUE. η_{out} (~$1/2n^2$) is the light out coupling efficiency (for glass substrates, n=1.5, η_{out} is estimated as ~20%), η_{rec} is the electron-hole recombination proportion, which is assumed to be 100%, η_{PL} is the quantum yield in the solid state, and η_s is the EUE

The **BPPI**-based devices exhibited excellent performance with a maximum current efficiency of ~1.34 cd A^{-1}, maximum power efficiency of ~1.40 lm W^{-1}, and maximum external quantum efficiency (EQE, ηext) of ~3.0%. Because the efficiency of **BPPI** in the solid state was measured to be ~85 % by deposition on the quartz plate using an integrating sphere apparatus, the EUE of **BPPI** in this device structure was about ~18.0% according to the relation equation between EQE and EUE shown in **Equation 2**. [22] **N-BPPI** exhibited a similar performance with a maximum current efficiency of ~1.38 cd A^{-1}, maximum power efficiency of ~0.96 lm W^{-1}, and maximum external quantum efficiency of ~2.0%. However, the efficiency of **N-BPPI** was only 30% in the film state, and the EUE was estimated to be ~33.0%, a value that exceeded the 25% limit of spin statistics, implying that the RISC process may be excited in the EL process. [4, 10]

The aforementioned device performance and EUE are not ideal, but the increasing EUE trend was obvious in the values from the *C2*-coupled D-A system to the *N1* system, which originated from the excited states change, with the stronger orbit coupling effect in **N-BPPI**. A similar result was also observed in TPM and TPMCN, and a detailed theoretical analysis was described in our previous report.[10a] Although the improvement of **N-BPPI** was lower than that of TPMCN, such a blue emitter with high solid efficiency is rare in non-doped deep-blue OLEDs. [3, 10b] Importantly, the EUE value not only gave us confidence that the *N1*-coupled D-A structure could improve the effective channel for triplet to singlet conversion as compared to the *C2*-coupled structure, but also indicated that appropriate CT components in excited states are necessary to balance the emission color, solid state efficiency and EUE

Table 3.. Summary of the device performance of **BPPI** and **N-BPPI**

Device	CIE [x, y][a]	Voltage [V][b]	LE Max [cd/A][c]	PE Max [lm/W][d]	L_{Max} [cd/m^2][e]	EQE (%)[f]	EUE (%)[g]
BPPI	0.15,0.13	3	1.34	1.40	3043	3.0	18
N-BPPI	0.15,0.08	4.5	1.38	0.96	139	2.0	33

[a] Taken at 9 V. [b] The turn-on voltage (L >1 cd/m^2). [c] The maximum values of luminance (LE_{max}). [d] The power efficiency (PE_{max}). [e] The maximum brightness (L_{max}). [f] External quantum efficiency (EQE). [g] exciton utilizing efficiency (EUE).

5. Conclusion

In summary, **BPPI** and **N-BPPI** were prepared by a one-pot chemical reaction and Suzuki coupling. They exhibited ideal thermal stabilities, higher fluorescence efficiencies, proper energy levels, and RISC characteristics. Their non-doped OLEDs showed deep blue emission with CIEs of (0.15, 0.13) and (0.15, 0.08) for **BPPI** and **N-BPPI**, respectively. Based on DFT calculations, photophysical analysis, and OLED performances, we derived the relationship between structure and property of the OLED. Although the groups substituted at the *N1* and *C2*-positions played important roles in the 3H-type non-doped blue emitters, there were some differences.

Specifically, in regard to the *C2*-coupling position:

(1) The transition direction of the LE and CT states were the same, and the emission color was very sensitive to the chemical structure at the *C2*-position.

(2) Because the oscillator strength of S_1 had the absolute advantage, these compounds exhibited higher fluorescence quantum yields.

(3) The energy barriers between neighboring excited states were higher and thus the conversion efficiency was limited.

In regard to the *N1*-coupling position:

(1) The transition directions of the LE and CT states were perpendicular.

(2) Because of the similar values at energy levels of S_1 to S_n, these materials exhibited higher nonradiative decay ratios and lower fluorescence quantum yields with relatively broad emission spectra, which influence the color purity in deep blue emitters.

(3) Owing to the stronger orbit coupling effect, the excited stated conversion channel was very efficient (such as RISC) and higher EUEs in the OLEDs were realized.

To prepare highly efficient, non-doped deep blue electroluminescent materials with better exciton utilizing efficiency, the *C2*-substituted group should offer a large enough orbital overlap of the LE state with sufficient oscillator strength and should ensure that the main peak is located in the deep blue region. On the other hand, the *N1*-substituted group should construct a weak CT state in order to control the decreased PL efficiency and broad emission spectra, and should provide an

efficient conversion channel for singlet excitons by RISC for enhancing EUE in OLEDs. These effects are consistent with those of most reported API derivatives. This work may offer operational guidance for non-doped deep blue electroluminescent materials based on APIs, although some details remain to be elucidated such as their donor and acceptor relationships.

Acknowledgements:

This work is financially supported by National Science Foundation of China (Grant No. 51203091, 60907013, 61377026), Liaoning Province Doctor Startup Fund (Grant No. 20131084) and Open Project of State Key Laboratory of Supramolecular Structure and Materials（sklssm201423）.

Notes and references

[a] *School of Petrochemical Engineering, Shenyang University of Technology, 30 Guanghua Street, Liaoyang, 111003, P. R. China Fax: +86 419 5319409; Tel: +86 419 5319409; E-mail: wangzhm1983@163.com*

[b] *State Key Laboratory of Supramolecular Structure and Materials, Jilin University, 2699 Qianjin Avenue, Changchun 130012,P.R.China.*

[c] *State Key Laboratory on Integrated Optoelectronics, College of Electronic Science and Engineering, Jilin University, 2699 Qianjin Avenue, Changchun 130012,P.R.China.*

† Electronic Supplementary Information (ESI) available: [details of any supplementary information available should be included here]. See DOI: 10.1039/b000000x/

‡Experimental: Pre*para*tion of **BPPI** and **N-BPPI**

A mixture of M1 or M2 (0.5 g, 1.12 mmol), 4,4,4',4',5,5,5',5'-octamethyl-2,2'-bi(1,3,2- dioxaborolane) (0.15 g, 0.56 mmol), $Pd(PPh_3)_4$ (25 mg, 0.03 mmol), and sodium carbonate (0.53 g, 5 mmol) in THF (20 mL) and distilled water (2.5 mL) was refluxed for 2 d under nitrogen. The crude product was concentrated by rotary evaporation and filtered. After drying at 40°C in a vacuum baking oven, the powder was purified by column chromatography.

BPPI : ^{1}H NMR (500 MHz, DMSO, ppm): 8.94 (d, J = 8.5 Hz ,2H), 8.89 (d, J = 8.2 Hz, 2H), 8.72 (d, J = 8.2 Hz, 2H), 7.80–7.65 (m, 22H), 7.57 (t, J = 7.9 Hz, 7.6Hz ,2H), 7.35 (t, J = 7.3 Hz,7.3Hz , 2H) , 7.09 (d, J = 8.2 Hz ,2H). MALDI-TOF (m/z): [M+] calcd. $C_{54}H_{34}N_4$, 738.28; found, 739.0. Anal Calc. for $C_{54}H_{34}N_4$: C, 87.78; H, 4.64; N, 7.58. Found: C, 87.80; H, 4.62; N, 7.57.

N-BPPI : ^{1}H NMR (500 MHz, DMSO, ppm): 8.98 (d, J = 8.9 Hz ,1H), 8.93 (d, J = 8.5 Hz, 1H), 8.73 (d, J = 7.6 Hz, 1H), 8.22 (d, J = 8.5 Hz, 2H), 7.92(d, J = 8.5 Hz, 2H), 7.78 (t, J = 7.6 Hz,7.4Hz , 1H), 7.72 (t, J = 8.6 Hz, 8.4Hz , 1H), 7.69-7.66 (m, 2H), 7.61 (t, J = 7.1 Hz,7.7Hz , 1H), 7.47-7.41 (m, 4H), 7.33 (d, J = 7.7 Hz ,1H). MALDI-TOF (m/z): [M+] calcd. $C_{54}H_{34}N_4$, 738.28; found, 739.0. Anal Calc. for $C_{54}H_{34}N_4$: C, 87.78; H, 4.64; N, 7.58. Found: C, 87.76; H, 4.62; N, 7.55.

1. a) C. W. Tang, S. A. VanSlyke, *Appl. Phys. Lett.* **1987**, *51*, 93; b) Y. G. Ma, H. Zhang, J. C. Shen, C. Che, *Synth. Met.* **1998**, *94*, 245; c) C. Adachi, M. A. Baldo, S. R. Forrest, M. E. Thompson, *J. Appl. Phys.* **1999**, *11*, 285; d) Y. Cao, I. D. Parker, G. Yu, C. Zhang, A. J. Heeger, *Nature*, **1998**, *397*, 414.
2. a) S. J. Su, E. Gonmori, H. Sarabe, J. Kido, *Adv. Mater.* **2008**, *20*, 4189; b) F. M. Hsu, C.H. Chien, C. F. Shu, C. H. Lai, C. C. Hsieh, K. W. Wang, P. T. Chou, *Adv. Funct. Mater.* **2009**, *19*, 2834; c) Y. Tao, Q. Wang, C. L. Yang, C. Zhong, K. Zhang, J. G. Qin, D. G. Ma, *Adv. Funct. Mater.* **2010**, *20*, 304; d) S. O. Jeon, S. E. Jang, H. S. Son, J. Y. Lee, *Adv. Mater.* **2011**, *23*, 1436.
3. M. R. Zhu, C. L. Yang, *Chem. Soc. Rev.*, **2013**, *42*, 4963.
4. a) C. J. Kuo, T. Y. Li, C. C. Lien, C. H. Liu, F. I. Wu, M. J. Huang, *J. Mater. Chem.*, **2009**, *19*, 1865; b) C. H. Cheng, C. H. Liu, F. I. Wu, **2010**, *U.S. Patent* No. 20100253208.
5. a) Z. M. Wang, P. Lu, S. M. Chen, Z. Gao, F. Z. Shen, W. S. Zhang, Y. X. Xu, H. S. Kwok and Ma Y. G. *J. Mater. Chem.*, **2011**, *21*, 5451; b) Z. M. Wang, Z. Gao, S. F. Xue, Y. L. Liu, W. S. Zhang, C. Gu, F. Z. Shen, P. Lu, Y. G. Ma, *Polym. Bull*, **2012**, *69*, 273; c) Z. M. Wang, X. H. Song, Z. Gao, D. W. Yu, X. J. Zhang, P. Lu, F. Z. Shen, Y. G. Ma, *RSC Adv.*, **2012**, *2*, 9635. d) Z. Wang, Y. Feng, H. Li, Z. Gao, X. Zhang, P. Lu, P. Chen, Y. Ma, S. Liu; *Phys. Chem. Chem. Phys,* **2014**, CP-ART-01-2014-000209.R2
6. a) Z. Gao, G. Cheng, F. Shen, S. Zhang, Y. Zhang, P. Lu1, Y. Ma, *Laser Photon. Rev.,* **2014**, *8*, L6; b) Z. Gao, Y. L. Liu, Z. M.Wang, F. Z. Shen, H. Liu, G. N. Sun, L. Yao, Y. Lv, P. Lu, Y. G. Ma, *Chem. Eur. J.* , **2013**, *19*, 2602.
7. a) Y. Yuan, D. Li, X. Q. Zhang, X. J. Zhao, Y. Liu, J. Y. Zhang, Y. Wang, *New J. Chem.*, **2011**, *35*, 1534; b) K. Wang, F. C. Zhao, C. G. Wang, S. Y. Chen, D. Chen, H. Y. Zhang, Y. Liu, D. G. Ma, Y. Wang, *Adv. Funct. Mater.*, **2013**, *23*, 2672; (c) H. Huang, Y. X Wang, S. Q. Zhuang, X. Yang, L. Wang, C. L. Yang, *J. Phys. Chem. C*, **2012**, *116*, 19458; d) S. Zhuang, R. Shangguan, H. Huang, G. Tua, L. Wana, X. Zhu, *Dyes Pigments*, **2014**, *101,* 93.
8. a) Y. Zhang, S. L. Lai, Q. X. Tong, M. F. Lo, T. W. Ng, M. Y Chan, Z. C. Wen, J. He, K. S. Jeff, X. L. Tang, W. M. Liu, C. C. Ko, P. F. Wang, C. S. Lee, *Chem. Mater*., **2012**, *24*, 61; b) Y. Zhang, S. L. Lai, Q. X. Tong, M. Y. Chan, T. W. Ng, Z. C. Wen, G. Q. Zhang, S. T. Lee, H. L. Kwong, C. S. Lee, *J. Mater. Chem.*, **2011**, *21*, 8206; c)Y. Yuan, J. Chen, F. Lu, Q. Tong, Q. Yang, H. Mo, T. Ng, F. Wong, Z. Guo, J. Ye, Z. Chen, X. Zhang, C. Lee, *Chem. Mater.*, 2013, *25*, 4957.
9. a) S. Q. Zhuang, R. G. Shangguan, J. J Jin, G. L. Tu, L. Wang, J. S. Chen, D. G. Ma, X. Ji Zhu, *Org. Electro.*, **2012**, *13*, 3050; b)J. L. Wang, W. Y. Lin, W. L. Li, *Biomater.*, **2013**, ***34***, 7429; c) X. Y. Zhang, J. Lin, X. H. Ouyang, Y. Liu, X. Y. Liu, Z. Y. Ge, *J. Photochem. Photobiol. A*, **2013**, *268*, 37; d) X. Ouyang, D. Chen, S. Zeng, X. Zhang, S. Su, Z. Ge, *J. Mater. Chem.,* **2012,** *22*, 23005; e) D. Kumar, K. R. J. Thomas, C. Lin, J. Jou, *Chem. Asian J.*, **2013**, *8*, 2111.
10. a) W. J. Li, D. D. Liu, F. Z. Shen, D. G. Ma, Z. M. Wang, T. Feng, Y. X. Xu, B. Yang, Y. G. Ma. *Adv. Funct. Mater.* **2012**, *22*, 2797; b) S. T. Zhang, W. J. Li, L. Yao, Y. Y. Pan, B. Yang,Y. G. Ma, *Chem. Commun.* **2013**, *49*, 11302; c) S. Tang, W. J. Li, F. Z. Shen, D. D. Liu, B. Yang, Y. G. Ma, *J. Mater. Chem*. **2012**, *22*, 4401; d) L. Yao, S. T. Zhang, R. Wang, W. J. Li, F. Z. Shen, B. Yang, Y. G. Ma, *Angew. Chem. Int. Ed.* **2014**, *53*, 2119; e) B. Yang, Y. G. Ma, *Sci. China Ser B* **2013**, 43, 1457.
11. a) K. Goushi, K. Yoshida, K. Sato, and C. Adachi, *Nature Photonics*, **2012**, *6*, 253; b) S. Reineke, M. A. Baldo, *Phys. Status. Solidi A*, 209, **2012**, 12, 2341; c) A. P. Monkman, *ISRN Mater. Sci.*, **2013**, 1-19. doi:10.1155/2013/670130; d) M. Segal, M. Singh, K. Rivoire, S. Difley, T. V. Voorhis, M. A. Baldo, *Nature Mater.,* **2007**, *6*, 374; e) S. Difley, D. Beljonne, T. V. Voorhis, *J. Am. Chem. Soc*., **2008**, *130*, 3420.
12. a) M. Pope, C. E. Swenberg, Electronic Processes in Organic Crystals and Polymers. Oxford University Press, **1999**; b) M. Segal, M. Singh, K. Rivoire, S. Difley, T. V. Voorhis, and M. A. Baldo, *Nature Mater.*, **2007**, *6*, 374; c) S. Difley, D. Beljonne, T. V. Voorhis, J. *Am. Chem. Soc*.,**2008**, *130*, 3420.
13. a) W. J. Li, Y. Y. Pan, R. Xiao, Q. M. Peng, S. T. Zhang, D. G. Ma, F. Li, F. Z. Shen, Y. H. Wang, B. Yang, Y. G. Ma, *Adv. Funct. Mater.*, **2013**, *24*, 1609; (b)Y. Pan, W. Li, S. Zhang, L. Yao, C. Gu1, H. Xu, B. Yang, Y. Ma, *Adv. Opt. Mater.* **2014** DOI: 10.1002/adom.201300467.
14. a) S. Tang, M. R. Liu, P. Lu, H. Xia, M. Li, Z. Q. Xie, F. Z. Shen, C. Gu, H. Wang, B. Yang, Y. G. Ma, *Adv. Funct. Mater.*, **2007**, *17*, 2869; b) C. Poriel, J. J. Liang, J. Rault-Berthelot, F. Barrire, N. Cocherel, A. M. Z. Slawin, D. Horhant, M. Virboul, G. Alcaraz, N. Audebrand, L. Vignau, N. Huby, G. Wantz, L. Hirsch, *Chem. Eur. J.*, **2007**, *13*, 10055; c) M. Santra, H. Moon, M. H. Park, T.-W. Lee, Y. K Kim, K. H. Ahn, *Chem. Eur. J.*, **2012**, *18*, 9886; d) H. Liu, P.

Chen, D. Hu, X. Tang, Y. Pan, H. Zhang, W. Zhang, X. Han, Q. Bai, P. Lu, Y. Ma, *Chem. Eur. J*., **2014**, *20*, 2149.

15. a) W. Zhiming, S. Xiaohui, L. Hui, F. Ying, L. Ping, Chem. *J. Chinese Univ*., **2014**, *35*, 505; b) Y. T. Chang, S. L. Hsu, G. Y. Chen, M. H. Su, T. A. Singh, E. W. G. Diau and K. H. Wei, *Adv. Funct. Mater.*, **2008**, *18*, 1; c) Y. T. Chang, S. L. Hsu, M. H. Su and T. K. H. Wei, *Adv. Funct. Mater.*, **2007**, *17*, 3326.
16. Z. Wang, Z. Gao, Y. Feng, Y. Liu, B. Yang, D. Liu, Y. Lv, P. Lu, Y. Ma, *Polymer*, **2013**, *54*, 6191.
17. a) Z. M. Wang, X. H. Song, L. L Ma, Y. Feng, C. Gu, X. J. Zhang, P. Lu, Y. G. Ma, *New J. Chem*., **2013**, *37*, 2440; b) Z. Wang, P. Lu, S. Xue, C. Gu, Y. Lv., Q. Zhu, H. Wang, Y. Ma., *Dyes Pigments*, **2011**, *91*, 356.
18. a) B. Yang, S. K. Kim, H. Xu, Y. I. Park, H. Zhang, C. Gu, F. Z. Shen, C. L. Wang, D. D. Liu, X. D. Liu, M. Hanif, S. Tang, W. J. Li, F. Li, J. C. Shen, J. W. Park, Y. G. Ma, *Chem. Phys. Chem*. **2008**, *9*, 2601; b) S. K. Kim, B. Yang, Y. G. Ma, J. H. Lee, J. W. Park. *J. Mater. Chem*. **2008**, *18*, 3376; c) S. K. Kim, B. Yang, Y. I. Park, Y. G. Ma, J. Y. Lee, H. J. Kim, J. Park, *Org. Electron*. **2009**, *10*, 822.
19. a) Z. R. Grabowski, K. Rotkiewicz, W. Rettig, *Chem. Rev.*, **2003**, *103*, 3899; b) Z. R. Grabowski, Rotkiewicz, E. Acta Phys. Polon. **1978**, *54A*, 767.
20. a) M. J. Frisch, et al. Gaussian 09, revision A.02, Gaussian, Inc., Wallingford CT, 2009; b) T. Yanai, D. P. Tew, N. C. Handy, *Chem. Phys. Lett.* **2004**, *393*, 51; c) T. Yanai, R. J.Harrison, N. C. Handy, *Mol. Phys.* **2005**, *103*, 413; c) Lippert,et. al. In Advances in Molecular Spectroscopy; Mangini, A., 95 Ed.; Pergamon Press: Oxford, 1962; p 443.
21. a) P. Chen, W. F. Xie, J. Li, T. Guan, Y. Duan, Y. Zhao, S. Y. Liu, C. S. Ma, *Appl. Phys. Lett.*, **2007**, *91*, 023505; b) P. Chen, Q. Xue, W. F. Xie, Y. Duan, G. H. Xie, Y. Zhao, J. Y. Hou, S. Y. Liu, L. Y. Zhang, B. Li, *Appl. Phys. Lett.*, **2008** *93,* 153508; c) P. Chen, Q. Xue, W. F. Xie, Y. Duan, G. H. Xie, Y. Zhao, J. Y. Hou, S. Y Liu, L. Y. Zhang, B. Li, *Appl. Phys. Lett.*, **2009**, *95*, 123307.
22. a) C. Adachi, M. A. Baldo, S. R. Forrest, M. E. Thompson, *J. Appl. Phys*. **1999**, *11*, 285; b) N. C. Greenham, R. H. Friend, D. D. C. Bradley, *Adv. Mater*. **1994**, *6*, 491.